

# A Site-Resolved 2D Quantum Simulator with Hundreds of Trapped Ions under Tunable Couplings

S.-A. Guo,<sup>1</sup> Y.-K. Wu,<sup>1,2</sup> J. Ye,<sup>1</sup> L. Zhang,<sup>1</sup> W.-Q. Lian,<sup>3</sup> R. Yao,<sup>3</sup> Y. Wang,<sup>1,3</sup> R.-Y. Yan,<sup>1</sup> Y.-J. Yi,<sup>1</sup> Y.-L. Xu,<sup>1</sup> B.-W. Li,<sup>3</sup> Y.-H. Hou,<sup>1</sup> Y.-Z. Xu,<sup>1</sup> W.-X. Guo,<sup>3</sup> C. Zhang,<sup>1</sup> B.-X. Qi,<sup>1</sup> Z.-C. Zhou,<sup>1,2</sup> L. He,<sup>1,2</sup> and L.-M. Duan<sup>1,2,4,\*</sup>

<sup>1</sup>*Center for Quantum Information, Institute for Interdisciplinary Information Sciences, Tsinghua University, Beijing 100084, PR China*

<sup>2</sup>*Hefei National Laboratory, Hefei 230088, PR China*

<sup>3</sup>*HYQ Co., Ltd., Beijing 100176, PR China*

<sup>4</sup>*New Cornerstone Science Laboratory, Beijing 100084, PR China*

A large qubit capacity and an individual readout capability are two crucial requirements for large-scale quantum computing and simulation. As one of the leading physical platforms for quantum information processing, the ion trap has achieved quantum simulation of tens of ions with site-resolved readout in 1D Paul trap, and that of hundreds of ions with global observables in 2D Penning trap. However, integrating these two features into a single system is still very challenging. Here we report the stable trapping of 512 ions in a 2D Wigner crystal and the sideband cooling of their transverse motion. We demonstrate the quantum simulation of long-range quantum Ising models with tunable coupling strengths and patterns, with or without frustration, using 300 ions. Enabled by the site resolution in the single-shot measurement, we observe rich spatial correlation patterns in the quasi-adiabatically prepared ground states. This spatial resolution further allows us to verify quantum simulation results by comparing with the calculated collective phonon modes. Our work paves the way for simulating classically intractable quantum dynamics and for running NISQ algorithms using 2D ion trap quantum simulators. With the further development of 2D individual addressing, our work also makes a building block for a large-scale ion trap quantum computer.

Quantum computation and quantum simulation have entered an era of hundreds of qubits [1–3], with complicated computational tasks beyond the reach of current classical computers being demonstrated [4–7]. To further extend the application of the noisy intermediate-scale quantum (NISQ) devices on practical and classically intractable problems, the quantum simulation of many-body dynamics [8] and the NISQ algorithms [9] like quantum annealing [10] and variational quantum algorithms [11] have attracted wide research interest. Apart from a large qubit number, a critical requirement for these applications is the ability to read out individual qubit states in a single shot [12], thus allowing, e.g., the measurement of qubits’ spatial correlation under quantum dynamics, or the evaluation of many-body objective functions in an optimization problem.

As one of the leading quantum computing platforms, the ion trap has demonstrated quantum simulation of up to 61 qubits in a 1D Paul trap with individual detection [13–15]. To further scale up the qubit number, one plausible way is to trap the ions in a 2D crystal. To date, 2D crystals of about 150 ions under Doppler cooling [16], of about 50 ions using two-tone laser cooling [17], and of about 100 ions under EIT cooling [18] have been reported, and the global quantum manipulation and individual detection have also been demonstrated with up to 10 ions in 2D [19]. Incidentally, 2D micro-trap arrays have also been achieved in the small scale with large inter-site distances and weak coupling strength [20–22], and 2D junctions for the quantum charge-coupled device (QCCD) architecture [23, 24] have also been realized as

a plausible way to scale up the system [25–27]. On the other hand, 2D ion crystals are native in Penning trap with quantum simulation of about 200 ions already being achieved [3, 28]. However, due to the fast rotation of the ion crystal in a Penning trap, the individual detection of qubit states remains an experimental challenge. Although spatial and temporal resolved imaging techniques have been used to count the ion number [3, 28], observables for quantum simulation in Penning trap are still limited to be global.

Here, we report the stable trapping of a 2D ion crystal of 512  $^{171}\text{Yb}^+$  ions with its relevant transverse modes (perpendicular to the ion plane) EIT and sideband cooled to below one phonon per mode. We have exact control of the ion numbers in the crystal and can set it to any desired value. We further use the spin-dependent AC Stark shift of 411 nm laser to generate long-range Ising coupling, and demonstrate the quantum simulation of the long-range quantum Ising model using 300 ions with tunable coupling patterns. Note that comparable qubit numbers have also been achieved for neutral atoms [1] and for superconducting circuits [2] with individual-qubit resolution. In these systems, qubits mainly possess short-range nearest-neighbor interactions, while trapped ions naturally host long-range spin interactions with tunable coupling range and patterns. Due to this unprecedented control of coupling patterns, rich exotic spatial correlations can be expected. In particular, by tuning the laser close to individual phonon sidebands and quasi-adiabatically preparing the ground states via slow ramping of parameters, we observe various spin-spin spatial correlation pat-

terns in which the collective oscillation modes of the ions are imprinted. By simultaneously coupling to multiple phonon modes, we further obtain frustrated Ising coupling that can find applications in classically intractable problems.

## STABLE TRAPPING OF 2D ION CRYSTALS

We use a monolithic 3D ion trap at the temperature of  $T = 6.1$  K to hold the large 2D ion crystal. The cryogenic temperature is crucial for suppressing the collision influence with the background gas molecules and for the stability of the 2D crystal. By adjusting the voltages on the  $4 \times 7$  DC electrodes, we shape the crystal of  $N = 512$  ions into roughly an ellipse with 11 rows, while minimizing the micromotion perpendicular to the plane, as shown in Fig. 1. The average distance between ions is about  $a \approx 4 \mu\text{m}$ . Global 370 nm laser beams for Doppler cooling, EIT cooling, optical pumping and state detection are shined along the  $yz$  plane so as to be immune to the micromotion of the ions in the  $x$  direction. Owing to the coupling of the  $x$  and  $z$  directions in the in-plane motion, such cooling beams are sufficient to cool down the  $x$  oscillation modes as well.

We further use a narrow-band global 411 nm laser in the  $y$  direction to provide sideband cooling for the transverse modes. For  $N = 512$  ions under the transverse trap frequency  $\omega_y = 2\pi \times 2.164$  MHz, the spectrum of the transverse modes spans about  $2\pi \times 1.25$  MHz below the center-of-mass (COM) mode. We perform sideband cooling to the highest  $2\pi \times 150$  kHz range by cooling 10 frequencies, which covers all the phonon modes relevant to the following quantum simulation experiments. The red and blue motional sideband spectra for the highest 5 modes are shown in Fig. 1d and e under Doppler cooling (blue) and sideband cooling (red). To estimate the phonon number from these spectra, we maintain a low excitation rate for each phonon mode [29], which results in the sensitivity to the state-preparation-and-measurement (SPAM) errors and the statistical fluctuation. Nevertheless, the current results allow us to bound the average phonon number to be below one phonon per mode, which is sufficient for our later quantum simulation of the spin model [30, 31]. More details about the setup, the daily operations and the estimation of the average phonon number can be found in Supplementary Information.

## QUANTUM SIMULATION OF LONG-RANGE ISING MODEL

We further perform quantum simulation on a crystal of  $N = 300$  ions, which supports higher Ising coupling strength through narrower 411 nm global beams. As

shown in Fig. 1b, the Ising model Hamiltonian is achieved by the spin-dependent force from counter-propagating off-resonant 411 nm laser beams [32] with the phonon states adiabatically eliminated. Here because the laser beams only couple  $|0\rangle \equiv |S_{1/2}, F = 0, m_F = 0\rangle$  to the  $D_{5/2}$  levels but not  $|1\rangle \equiv |S_{1/2}, F = 1, m_F = 0\rangle$ , the Ising Hamiltonian takes the form of

$$\begin{aligned} H_0 &= \sum_{ij} J_{ij} (I + \sigma_z^i) (I + \sigma_z^j) \\ &\equiv \sum_{i \neq j} J_{ij} \sigma_z^i \sigma_z^j + \sum_i h_i \sigma_z^i, \end{aligned} \quad (1)$$

where we have dropped an irrelevant constant. Apart from when coupling to the COM mode, the longitudinal field  $h_i \equiv 2 \sum_j J_{ij}$  is typically small (see Supplementary Information for details), and can further be compensated by a time-independent AC Stark shift of the 411 nm laser.

A transverse field  $H_B = B \sum_i \sigma_x^i$  can be realized by a global microwave resonant to the qubit frequency. As shown in Fig. 1f, we initialize all the qubits in  $|+\rangle \equiv (|0\rangle + |1\rangle)/\sqrt{2}$  (prepared by the SK1 composite pulse to suppress the microwave inhomogeneity) and slowly ramp down the transverse field following an exponential path  $B(t) = B_0 e^{-t/\tau}$ . By choosing  $B_0 > 5J_0$  where  $J_0 \equiv \frac{1}{N} \sum_{i \neq j} J_{ij}$  is the Kac normalized coupling strength, we start from the highest eigenstate of the Hamiltonian  $H(t) = H_0 + H_B(t)$ . We further choose a total evolution time  $T > 5\tau$ , and expect the final state to be close to the highest excited state of  $H_0$ , namely the ground state of  $-H_0$ .

Ideally when  $h_i = 0$ , the system possesses  $Z_2$  symmetry and we expect the final state to be invariant under the flip of all the spins. This shall give us large spin-spin correlation  $C_{ij} \equiv \langle \sigma_z^i \sigma_z^j \rangle - \langle \sigma_z^i \rangle \langle \sigma_z^j \rangle = \langle \sigma_z^i \sigma_z^j \rangle$  in the prepared ground state. Even with the small uncompensated  $h_i$ 's, the pattern in the spatial correlation still survives, as can be seen in Fig. 2. Specifically, if we couple dominantly to the COM mode with a positive detuning, it is well-known that  $-H_0$  is an all-to-all coupled ferromagnetic Ising model whose ground state shows long-range correlation  $C_{ij} = 1$ . This behavior can be observed in Fig. 2a where we obtain positive correlations over almost all the ion pairs. The deviation from the ideal value of one can come from the nonadiabatic excitation or decoherence during the slow quench, and the state detection error for individual qubits (we use electron shelving to suppress the detection error to be below 1% [33–35]), as is evident from Fig. 2b for the typical single-shot measurement outcomes. Besides, a reduced correlation can arise from a weak uncompensated longitudinal field, which will prefer one ferromagnetic ground state in Fig. 2b to the other, and thus increases the  $\langle \sigma_z^i \rangle \langle \sigma_z^j \rangle$  term. Similarly, in Fig. 2d and e we couple dominantly to the fourth highest phonon mode with a positive detuning, and observe a

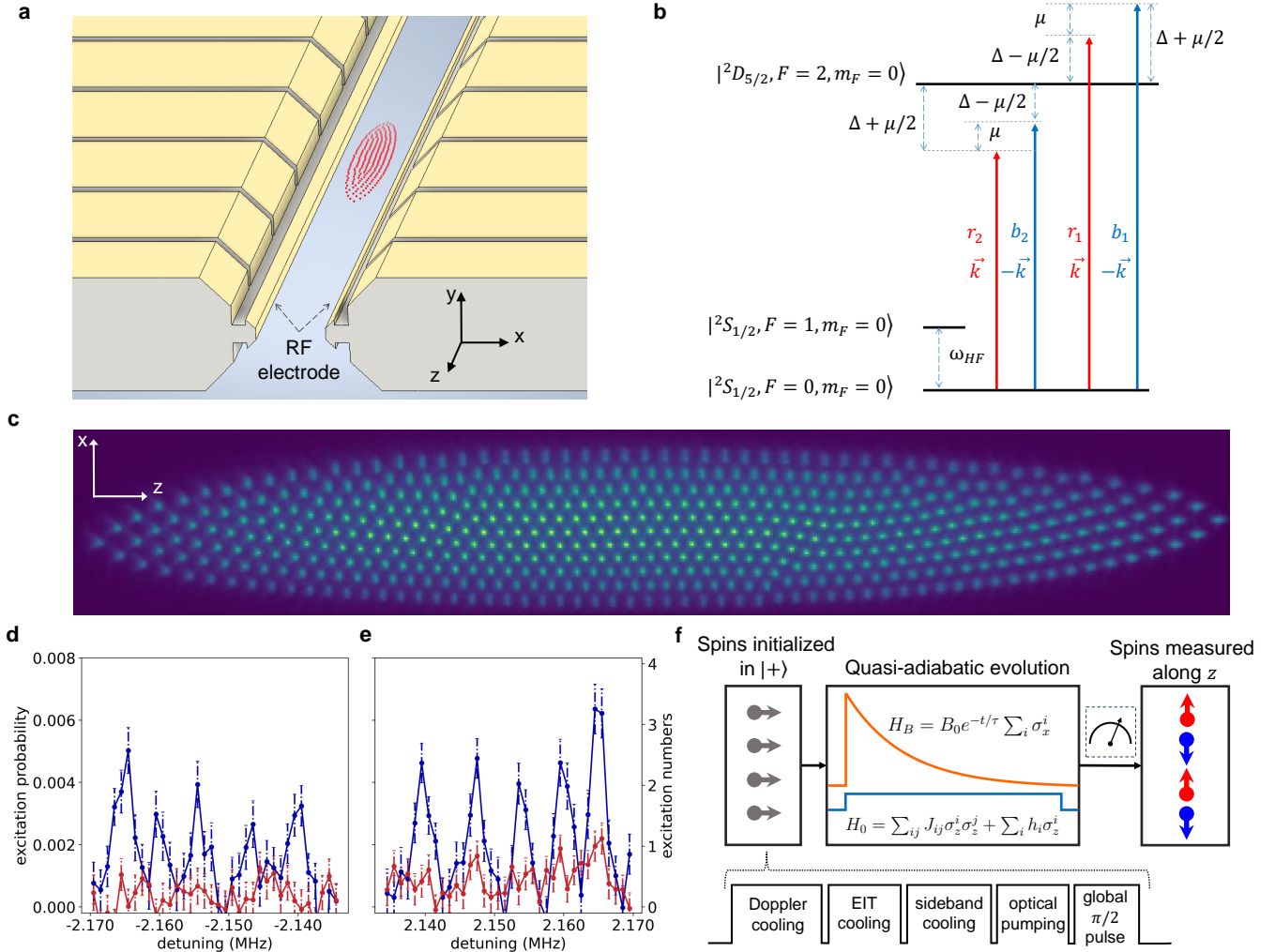


**FIG. 1. Experimental setup and 2D ion crystals.** **a**, An illustration of our monolithic 3D ion trap at cryogenic temperature. The 2D ion crystal locates on the  $xz$  plane and its size is not to scale. **b**, Relevant energy levels of the  $^{171}\text{Yb}^+$  ion. The qubit is encoded in the  $S_{1/2}$  hyperfine levels  $|0\rangle \equiv |F=0, m_F=0\rangle$  and  $|1\rangle \equiv |F=1, m_F=0\rangle$ , and can be rotated by a resonant global microwave. Counter-propagating off-resonant 411 nm laser beams are used to generate spin-dependent forces on the ions, which further lead to the effective Ising coupling when the phonon states are adiabatically eliminated. Two pairs of frequency components are placed on the two sides of the  $S$ - $D$  transition with detuning  $\pm(\Delta \pm \mu/2)$  to create a beat note of  $\mu$  while compensating their time-independent AC Stark shift. **c**, The image of a 2D ion crystal with  $N = 512$  ions. **d**, The spectrum of the red motional sideband of the transverse phonon modes and **e**, that of the blue motional sideband under Doppler cooling (blue) and sideband cooling (red). Here we only show the highest five modes including the center-of-mass (COM) mode, while the complete spectra can be found in Supplementary Information. **f**, The experimental sequence to quasi-adiabatically prepare the ground state of an Ising model Hamiltonian. We initialize all spins in  $|0\rangle$  after laser cooling and optical pumping, and then rotate them to  $|+\rangle$  by a global microwave SK1 composite  $\pi/2$  pulse. Then we turn on the Ising model Hamiltonian  $H_0$  via the global 411 nm laser and the transverse field  $H_B$  via the global microwave simultaneously, and we quench the strength of the transverse field from  $B_0 \gg J_0$  following an exponential path, where  $J_0 = \frac{1}{N} \sum_{i \neq j} J_{ij}$  is the Kac normalized coupling strength.

staggered spatial pattern. These spatial correlations can further be quantified in momentum space. As shown in Fig. 2c and f, we obtain a momentum of about 0 for the ferromagnetic ground state with all-to-all coupling, and a momentum of about  $k_z \approx 0.06\pi/a$  for the staggered case which corresponds to a spatial period of about  $30a$  where  $a \approx 4 \mu\text{m}$  is the average ion distance.

Actually, when coupled to a single mode  $k$ , the ground state can be solved analytically and is governed by the structure of the phonon mode. This can be understood by factoring the Hamiltonian in Eq. (1) after the sup-

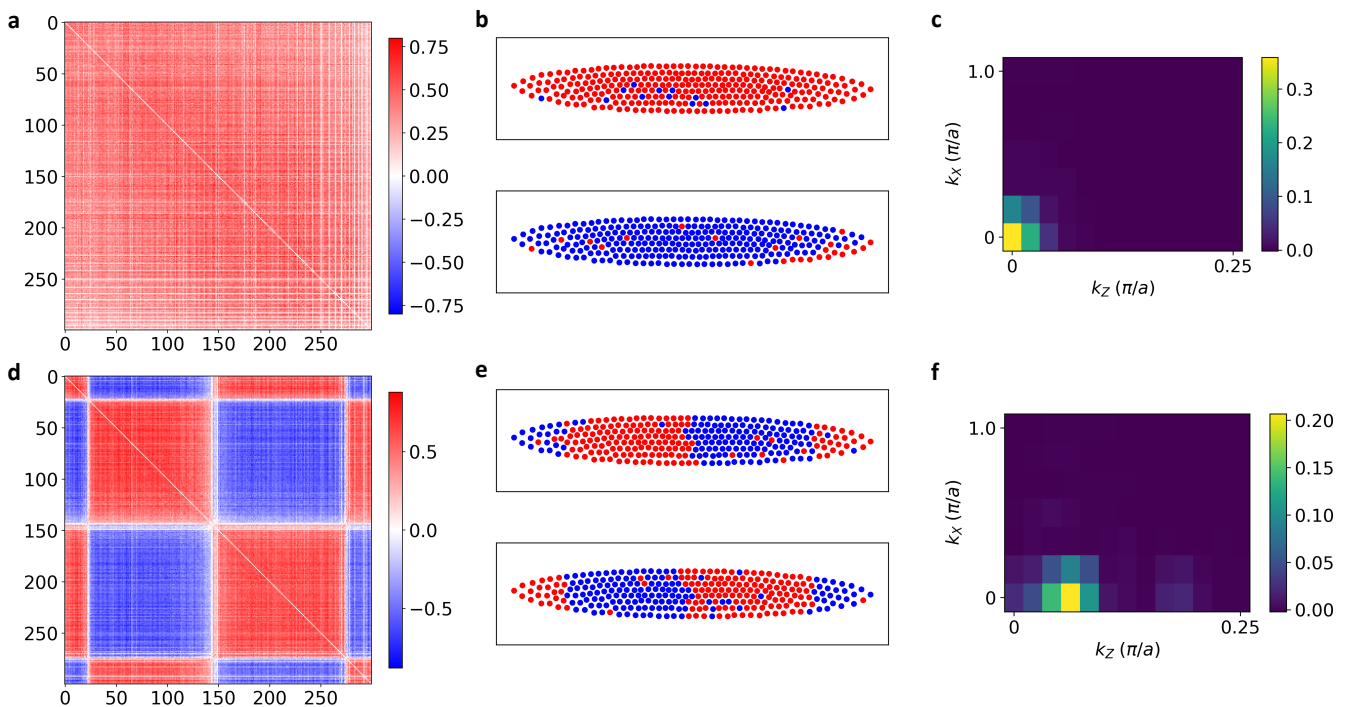


FIG. 2. **Spatial correlation patterns in quasi-adiabatically prepared ground states.** **a**, The covariance matrix between all the ion pairs  $C_{ij} \equiv \langle \sigma_z^i \sigma_z^j \rangle - \langle \sigma_z^i \rangle \langle \sigma_z^j \rangle$  (with the diagonal terms set to zero) when the beat note  $\mu$  of the 411 nm laser is detuned by  $\delta = \mu - \omega_1 = 2\pi \times 4$  kHz above the COM mode  $\omega_1 = \omega_y = 2\pi \times 2.138$  MHz. The  $N = 300$  ions are labelled in ascending order of their  $z$  coordinates. **b**, Typical single-shot measurement results for the state of  $N = 300$  qubits. The blue and the red dots represent  $|0\rangle$  and  $|1\rangle$ , respectively. Each ion can be resolved individually, and the overlap in the plot is due to the finite size of the markers. Small deviation from the ferromagnetic ground state comes from the nonadiabatic excitation and decoherence during the quench, as well as the detection error of the EMCCD. **c**, Fourier transform of the  $N(N - 1)$  directed pairs of correlations into the momentum space. The unit is  $\pi/a$  where  $a \approx 4 \mu\text{m}$  is the average ion distance. **d-f**, Similar plots when the beat note  $\mu$  of the 411 nm laser is detuned by  $\delta = \mu - \omega_4 = 2\pi \times 1$  kHz above the fourth highest phonon mode  $\omega_4 = \omega_y - 2\pi \times 24.0$  kHz. All the correlations are averaged over 100 samples.

pressing of the longitudinal field as

$$H_0 = \frac{1}{16\delta_k} \left( \sum_i \eta_k b_{ik} \Omega_i \sigma_z^i \right)^2, \quad (2)$$

where  $\delta_k$  is the detuning to the mode  $k$ ,  $\eta_k$  the Lamb-Dicke parameter,  $\Omega_i$  the 411 nm-laser-induced AC Stark shift on the ion  $i$ , and  $b_{ik}$  the normalized mode vector. Therefore when  $\delta_k > 0$ , the highest eigenstate of  $H_0$ , or the ground state of  $-H_0$ , can be simply expressed as  $\sigma_z^i = \pm \text{sign}(b_{ik})$ , thus imprinting the phonon mode structure into the observed spatial correlation.

Combining this classically solvable ground state and the spatial resolution, we can verify the quantum simulation result by comparing with the calculated phonon mode. In Fig. 3 we couple to a phonon mode with spatial structures both along the major and the minor axes of the ion crystal. The typical single-shot measurement result (Fig. 3a) agrees well with the theoretically calculated mode vector (Fig. 3b). We further show the average spin-spin correlation from 100 repetitions in Fig. 3d. Because of the 2D correlation pattern which is quantified in

the momentum space in Fig. 3c, the correlation appears to be noisy in Fig. 3d as we flatten the 2D structure into 1D in the rows and columns of the matrix. However, if we simply rearrange the indices of the ions into the descending order of  $b_{ik}$ , we obtain the matrix in Fig. 3e. Here we have two groups of ions with positive and negative  $b_{ik}$ 's, which explains the positive correlation within each group, and the negative correlation between them. Again, this verifies the agreement between the theoretical and the experimental results. Note that here when computing the phonon mode structure, we simply assume a harmonic trap and use the measured ion positions as the starting point to search the theoretical equilibrium configuration. This can be improved by fitting the anharmonicity over the large crystal using the measured transverse mode frequencies.

In all the above cases we couple dominantly to a single phonon mode with positive detuning, so that the Ising coupling shows no frustration and the ground state can be easily understood from the phonon mode structure. We further engineer frustrated Ising models in Fig. 4 by



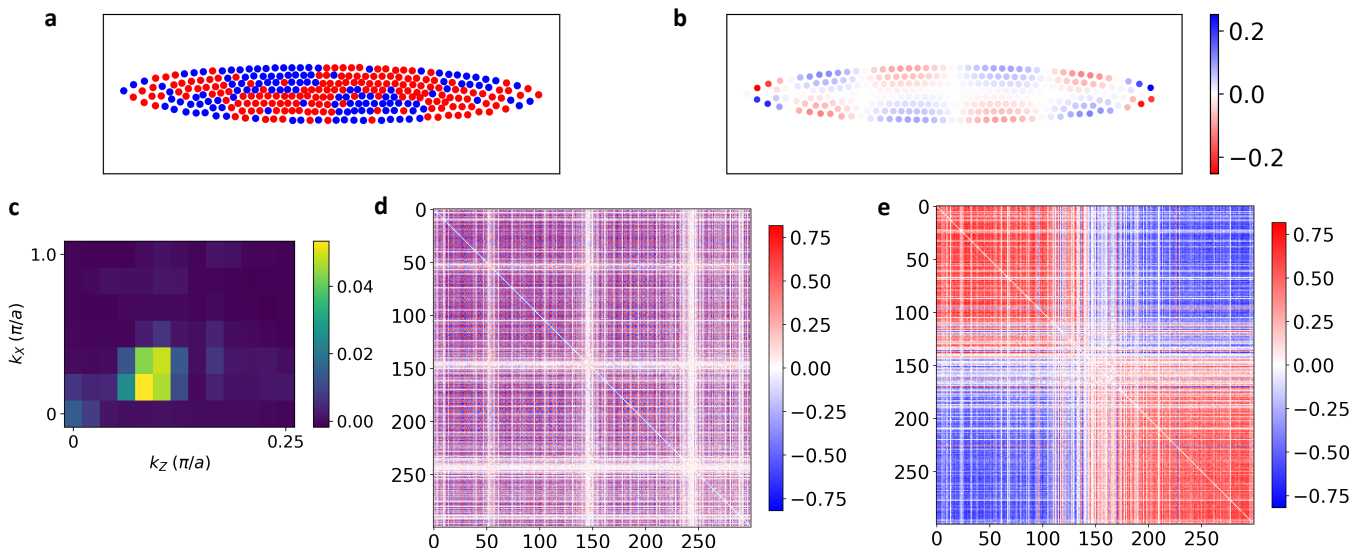


FIG. 3. **Verifying quantum simulation results by collective phonon modes.** **a**, Typical single-shot measurement result for the same  $N = 300$  crystal as Fig. 2 when the beat note  $\mu$  of the 411 nm laser is detuned by  $\delta = \mu - \omega_{19} = 2\pi \times 1$  kHz above the 19th highest phonon mode  $\omega_{19} = \omega_y - 2\pi \times 139.2$  kHz. **b**, Theoretically computed phonon mode structure  $b_{i,19}$  for the 19th mode assuming harmonic trap potentials in three spatial directions. **c**, Spin-spin correlation in momentum space. Nonzero momenta along both the  $x$  and the  $z$  axes can be seen. **d**, Experimentally measured covariance matrix when the ions are labelled in ascending order of their  $z$  coordinates. Since the correlations are oscillating both along the  $x$  and the  $z$  axes, when flattened into one axis, it is difficult to see the contiguous domains. **e**, The same covariance matrix as **d**, but with the ions rearranged in descending order of  $b_{i,19}$ . All the correlations are averaged over 100 samples.

coupling to more phonon modes simultaneously, or by setting a negative detuning. In Fig. 4a and b we show the spin-spin correlation when coupling to the mode 4 and the mode 7 individually. Then we couple to the two modes simultaneously via the two pairs of frequency components in the 411 nm laser in Fig. 1b. From Fig. 4c to e, we fix the detuning  $\delta_4$  to the mode 4 and increase the detuning  $\delta_7$  to the mode 7, such that their relative contribution to the Ising Hamiltonian changes. For small  $\delta_7 > 0$  (Fig. 4c), the mode 7 dominates and the correlation pattern is similar to Fig. 4b; for large  $\delta_7$  (Fig. 4e), the mode 4 dominates and the correlation pattern resembles Fig. 4a; while in the middle with roughly equal contribution from both modes, we see competition from the two patterns and the correlation becomes their mixture. From Fig. 4f to i, we increase both  $\delta_4$  and  $\delta_7$  from negative to positive. In Fig. 4h with  $\delta_4 = 2\pi \times 1.5$  kHz and  $\delta_7 = 2\pi \times 0.5$  kHz, the situation is similar to Fig. 4c dominated by the mode 7. If we further increase  $\delta_4$  and  $\delta_7$  to Fig. 4i, the generated Ising coupling decreases as well as the energy gap, making it more difficult to prepare the ground state adiabatically and thus the correlation also shrinks. On the other hand, if we decrease the detuning to  $\delta_4 = 2\pi \times 0.5$  kHz and  $\delta_7 = -2\pi \times 0.5$  kHz (Fig. 4g), the ground state becomes dominated by the mode 4 with positive detuning, but is also influenced by the weak frustrated Ising coupling from the negatively detuned mode 7. Finally, when both  $\delta_4$  and  $\delta_7$  are negative (Fig. 4f),

the Ising model becomes highly frustrated and the correlation in the slowly quenched state also becomes much weaker, with no simple analytical explanation for the observed pattern.

## DISCUSSION AND OUTLOOK

In this work, we achieve the stable trapping of a 2D crystal of above 500 ions, and demonstrate the quantum simulation of 300 ions with individual state detection. Currently this smaller ion number is chosen according to our available 411 nm laser power to cover the whole ion crystal for strong Ising coupling, and is not a fundamental limit. To further scale up the system to thousands of ions, we may also perform sympathetic cooling on a few ions with optimized locations [36] to maintain its stability, while using the dual-type qubit scheme to avoid crosstalk errors on the ions carrying quantum information as we have demonstrated recently in small systems [35].

We create frustrated Ising model Hamiltonian by coupling to up to two phonon modes. By adding more frequency components into the 411 nm laser [37, 38] or by applying a spatial gradient of the AC Stark shift [39], it will be possible to engineer more complicated coupling coefficients, and thus to simulate rich quantum dynamics that are intractable for classical computers [8] and to execute NISQ algorithms [9] like quantum annealing [10]

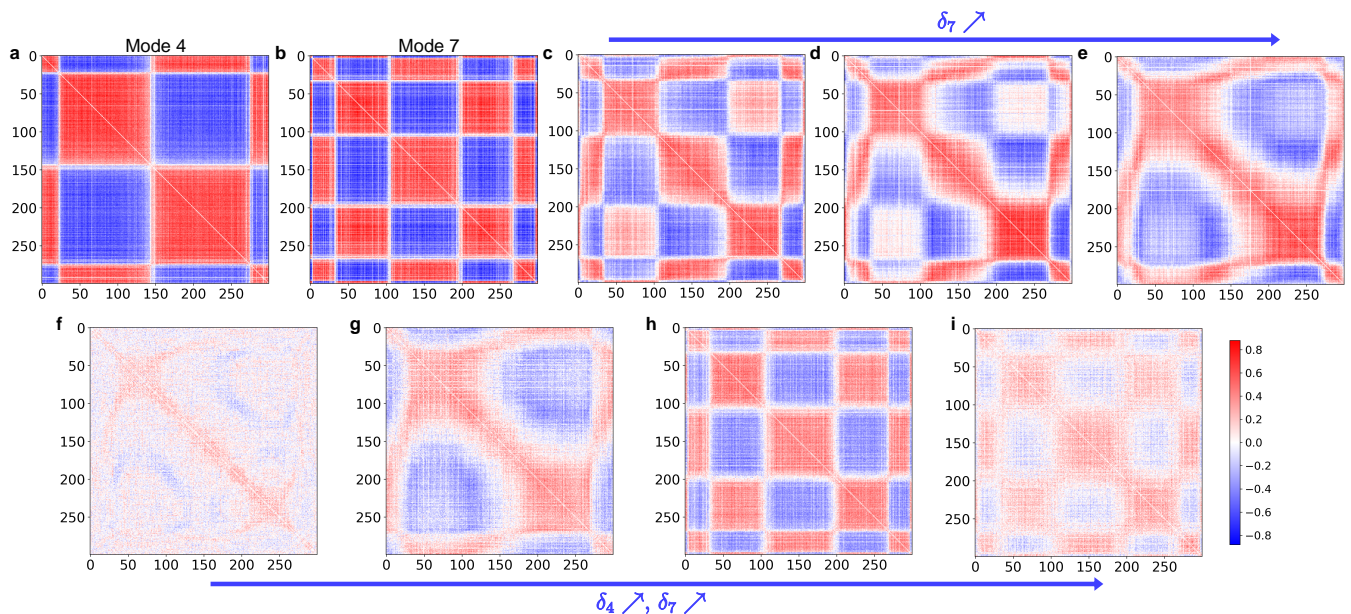


FIG. 4. **Quantum simulation of frustrated Ising model.** **a, b**, The covariance matrices for the same  $N = 300$  crystal as Fig. 2 when the beat note of the 411 nm laser is  $2\pi \times 1$  kHz above the 4th highest phonon mode and  $2\pi \times 1$  kHz above the 7th highest phonon mode, respectively. **c-e**, Two beat note frequencies of the 411 nm laser are applied to couple both phonon modes simultaneously. From left to right, we fix the detuning to the 4th mode as  $\delta_4 = 2\pi \times 0.75$  kHz, and increase the detuning to the 7th mode as  $\delta_7 = 2\pi \times [0.50, 0.75, 1.00]$  kHz. On the two ends, the ground states are dominated by the two modes, respectively, while in the middle there is frustration due to the competition between the two configurations. **f-i**, Again we couple both phonon modes simultaneously. From left to right, we increase the detunings to the two phonon sidebands simultaneously as  $(\delta_4, \delta_7)/2\pi = (-0.5, -1.5), (0.5, -0.5), (1.5, 0.5), (2.5, 1.5)$  kHz. When  $\delta_4, \delta_7 > 0$  (**h**), the ground state is dominated by the mode 7 under the chosen parameters, similar to **c**. When detunings further increase (**i**), the Ising coupling decreases, and so do the measured correlations due to the stronger nonadiabatic excitation. When  $\delta_4 > 0$  and  $\delta_7 < 0$  (**g**), the ground state is dominated by the mode 4, but also feels the frustrated Ising coupling from the mode 7 under negative detuning. Finally, when  $\delta_4, \delta_7 < 0$  (**f**), both contributions to the Ising coupling coefficients are strongly frustrated and it is difficult to theoretically predict the result. All the correlations are averaged over 100 samples.

and variational quantum optimization [11]. Furthermore, by integrating the 2D laser addressing into the system [40, 41], our 2D ion crystal can also support high-fidelity two-qubit entangling gates mediated by the transverse phonon modes [42, 43], thus largely extending the scale of ion trap quantum computers.

This work was supported by Innovation Program for Quantum Science and Technology (2021ZD0301601), Tsinghua University Initiative Scientific Research Program, and the Ministry of Education of China. L.M.D. acknowledges in addition support from the New Cornerstone Science Foundation through the New Cornerstone Investigator Program. Y.K.W. acknowledges in addition support from Tsinghua University Dushi program and the start-up fund.

\* [lmduan@tsinghua.edu.cn](mailto:lmduan@tsinghua.edu.cn)

[1] S. Ebadi, T. T. Wang, H. Levine, A. Keesling, G. Semeghini, A. Omran, D. Bluvstein, R. Samajdar, H. Pichler, W. W. Ho, *et al.*, *Nature* **595**, 227 (2021).

[2] Y. Kim, A. Eddins, S. Anand, K. X. Wei, E. Van Den Berg, S. Rosenblatt, H. Nayfeh, Y. Wu, M. Zaletel, K. Temme, *et al.*, *Nature* **618**, 500 (2023).  
 [3] J. G. Bohnet, B. C. Sawyer, J. W. Britton, M. L. Wall, A. M. Rey, M. Foss-Feig, and J. J. Bollinger, *Science* **352**, 1297 (2016).  
 [4] F. Arute, K. Arya, R. Babbush, D. Bacon, J. C. Bardin, R. Barends, R. Biswas, S. Boixo, F. G. Brandao, D. A. Buell, *et al.*, *Nature* **574**, 505 (2019).  
 [5] H.-S. Zhong, H. Wang, Y.-H. Deng, M.-C. Chen, L.-C. Peng, Y.-H. Luo, J. Qin, D. Wu, X. Ding, Y. Hu, P. Hu, X.-Y. Yang, W.-J. Zhang, H. Li, Y. Li, X. Jiang, L. Gan, G. Yang, L. You, Z. Wang, L. Li, N.-L. Liu, C.-Y. Lu, and J.-W. Pan, *Science* **370**, 1460 (2020).  
 [6] Y. Wu, W.-S. Bao, S. Cao, F. Chen, M.-C. Chen, X. Chen, T.-H. Chung, H. Deng, Y. Du, D. Fan, M. Gong, C. Guo, C. Guo, S. Guo, L. Han, L. Hong, H.-L. Huang, Y.-H. Huo, L. Li, N. Li, S. Li, Y. Li, F. Liang, C. Lin, J. Lin, H. Qian, D. Qiao, H. Rong, H. Su, L. Sun, L. Wang, S. Wang, D. Wu, Y. Xu, K. Yan, W. Yang, Y. Yang, Y. Ye, J. Yin, C. Ying, J. Yu, C. Zha, C. Zhang, H. Zhang, K. Zhang, Y. Zhang, H. Zhao, Y. Zhao, L. Zhou, Q. Zhu, C.-Y. Lu, C.-Z. Peng, X. Zhu, and J.-W. Pan, *Phys. Rev. Lett.* **127**, 180501 (2021).  
 [7] L. S. Madsen, F. Laudenbach, M. F. Askarani, F. Rortais,

- T. Vincent, J. F. Bulmer, F. M. Miatto, L. Neuhaus, L. G. Helt, M. J. Collins, *et al.*, *Nature* **606**, 75 (2022).
- [8] I. M. Georgescu, S. Ashhab, and F. Nori, *Rev. Mod. Phys.* **86**, 153 (2014).
- [9] K. Bharti, A. Cervera-Lierta, T. H. Kyaw, T. Haug, S. Alperin-Lea, A. Anand, M. Degroote, H. Heimonen, J. S. Kottmann, T. Menke, W.-K. Mok, S. Sim, L.-C. Kwek, and A. Aspuru-Guzik, *Rev. Mod. Phys.* **94**, 015004 (2022).
- [10] P. Hauke, H. G. Katzgraber, W. Lechner, H. Nishimori, and W. D. Oliver, *Reports on Progress in Physics* **83**, 054401 (2020).
- [11] M. Cerezo, A. Arrasmith, R. Babbush, S. C. Benjamin, S. Endo, K. Fujii, J. R. McClean, K. Mitarai, X. Yuan, L. Cincio, *et al.*, *Nature Reviews Physics* **3**, 625 (2021).
- [12] D. P. DiVincenzo, *Fortschritte der Physik* **48**, 771 (2000).
- [13] J. Zhang, G. Pagano, P. W. Hess, A. Kyprianidis, P. Becker, H. Kaplan, A. V. Gorshkov, Z.-X. Gong, and C. Monroe, *Nature* **551**, 601 (2017).
- [14] M. K. Joshi, F. Kranzl, A. Schuckert, I. Lovas, C. Maier, R. Blatt, M. Knap, and C. F. Roos, *Science* **376**, 720 (2022).
- [15] B.-W. Li, Y.-K. Wu, Q.-X. Mei, R. Yao, W.-Q. Lian, M.-L. Cai, Y. Wang, B.-X. Qi, L. Yao, L. He, Z.-C. Zhou, and L.-M. Duan, *PRX Quantum* **4**, 010302 (2023).
- [16] B. Szymanski, R. Dubessy, B. Dubost, S. Guibal, J.-P. Likforman, and L. Guidoni, *Applied Physics Letters* **100**, 171110 (2012).
- [17] A. Kato, A. Goel, R. Lee, Z. Ye, S. Karki, J. J. Liu, A. Nomerotski, and B. B. Blinov, *Phys. Rev. A* **105**, 023101 (2022).
- [18] D. Kiesenhofer, H. Hainzer, A. Zhdanov, P. C. Holz, M. Bock, T. Ollikainen, and C. F. Roos, *PRX Quantum* **4**, 020317 (2023).
- [19] M. Qiao, Z. Cai, Y. Wang, B. Du, N. Jin, W. Chen, P. Wang, C. Luan, E. Gao, X. Sun, H. Tian, J. Zhang, and K. Kim, arXiv preprint arXiv:2204.07283 (2022).
- [20] R. C. Sterling, H. Rattanasonti, S. Weidt, K. Lake, P. Srinivasan, S. Webster, M. Kraft, and W. K. Hensinger, *Nature communications* **5**, 3637 (2014).
- [21] P. Kiefer, F. Hakelberg, M. Wittemer, A. Bermúdez, D. Porras, U. Warring, and T. Schaetz, *Phys. Rev. Lett.* **123**, 213605 (2019).
- [22] P. C. Holz, S. Aughter, G. Stocker, M. Valentini, K. Lakhmanskiy, C. Rössler, P. Stampfer, S. Sgouridis, E. Aschauer, Y. Colombe, and R. Blatt, *Advanced Quantum Technologies* **3**, 2000031 (2020).
- [23] D. J. Wineland, C. Monroe, W. M. Itano, D. Leibfried, B. E. King, and D. M. Meekhof, *Journal of research of the National Institute of Standards and Technology* **103**, 259 (1998).
- [24] D. Kielpinski, C. Monroe, and D. J. Wineland, *Nature* **417**, 709 (2002).
- [25] J. M. Amini, H. Uys, J. H. Wesenberg, S. Seidelin, J. Britton, J. J. Bollinger, D. Leibfried, C. Ospelkaus, A. P. VanDevender, and D. J. Wineland, *New Journal of Physics* **12**, 033031 (2010).
- [26] G. Shu, G. Vittorini, A. Buikema, C. S. Nichols, C. Volin, D. Stick, and K. R. Brown, *Phys. Rev. A* **89**, 062308 (2014).
- [27] W. C. Burton, B. Estey, I. M. Hoffman, A. R. Perry, C. Volin, and G. Price, *Phys. Rev. Lett.* **130**, 173202 (2023).
- [28] J. W. Britton, B. C. Sawyer, A. C. Keith, C.-C. J. Wang, J. K. Freericks, H. Uys, M. J. Biercuk, and J. J. Bollinger, *Nature* **484**, 489 (2012).
- [29] B.-W. Li, Q.-X. Mei, Y.-K. Wu, M.-L. Cai, Y. Wang, L. Yao, Z.-C. Zhou, and L.-M. Duan, *Phys. Rev. Lett.* **129**, 140501 (2022).
- [30] A. Sørensen and K. Mølmer, *Phys. Rev. Lett.* **82**, 1971 (1999).
- [31] K. Kim, M.-S. Chang, R. Islam, S. Korenblit, L.-M. Duan, and C. Monroe, *Phys. Rev. Lett.* **103**, 120502 (2009).
- [32] C. H. Baldwin, B. J. Bjork, M. Foss-Feig, J. P. Gaebler, D. Hayes, M. G. Kokish, C. Langer, J. A. Sedlacek, D. Stack, and G. Vittorini, *Phys. Rev. A* **103**, 012603 (2021).
- [33] C. Roman, A. Ransford, M. Ip, and W. C. Campbell, *New Journal of Physics* **22**, 073038 (2020).
- [34] C. L. Edmunds, T. R. Tan, A. R. Milne, A. Singh, M. J. Biercuk, and C. Hempel, *Phys. Rev. A* **104**, 012606 (2021).
- [35] H.-X. Yang, J.-Y. Ma, Y.-K. Wu, Y. Wang, M.-M. Cao, W.-X. Guo, Y.-Y. Huang, L. Feng, Z.-C. Zhou, and L.-M. Duan, *Nature Physics* **18**, 1058 (2022).
- [36] Z.-C. Mao, Y.-Z. Xu, Q.-X. Mei, W.-D. Zhao, Y. Jiang, Y. Wang, X.-Y. Chang, L. He, L. Yao, Z.-C. Zhou, Y.-K. Wu, and L.-M. Duan, *Phys. Rev. Lett.* **127**, 143201 (2021).
- [37] S. Korenblit, D. Kafri, W. C. Campbell, R. Islam, E. E. Edwards, Z.-X. Gong, G.-D. Lin, L.-M. Duan, J. Kim, K. Kim, and C. Monroe, *New Journal of Physics* **14**, 095024 (2012).
- [38] Q. Wu, Y. Shi, and J. Zhang, arXiv preprint arXiv:2308.10179 (2023).
- [39] Y. Shapira, T. Manovitz, N. Akerman, A. Stern, and R. Ozeri, *Phys. Rev. X* **13**, 021021 (2023).
- [40] Y. Pu, N. Jiang, W. Chang, H. Yang, C. Li, and L. Duan, *Nature communications* **8**, 15359 (2017).
- [41] Y. Wang, S. Crain, C. Fang, B. Zhang, S. Huang, Q. Liang, P. H. Leung, K. R. Brown, and J. Kim, *Phys. Rev. Lett.* **125**, 150505 (2020).
- [42] S.-T. Wang, C. Shen, and L.-M. Duan, *Scientific reports* **5**, 8555 (2015).
- [43] Y.-K. Wu, Z.-D. Liu, W.-D. Zhao, and L.-M. Duan, *Phys. Rev. A* **103**, 022419 (2021).